Theodore Langhorst[1], Tamlin Pavelsky[1]

[1]University of North Carolina at Chapel Hill, Department of Earth, Marine and Environmental Sciences. Chapel Hill, NC, USA.

Corresponding author: Theodore Langhorst (`tlang@live.unc.edu`)

Key Points:

- We developed the first global dataset of riverbank erosion and accretion for rivers wider than 150m.

- We confirm that regional first order relationships between river size and riverbank erosion apply globally.

- We show large interbasin differences in riverbank erosion that arise from the unique geography of each river basin.

Abstract

Riverbank migration has historically been seen as a risk to infrastructure that can be combatted through channelization, bank stabilization, and sediment trapping. The physical processes involved with riverbank erosion and deposition are well defined, yet the solutions to these equations are computationally and data intensive over large domains. While current understanding of large-scale river channel mobility largely comes from reach- and watershed-scale observations, we need global observations of riverbank erosion and accretion to understand sediment processes within and across river basins. In this work, we create the first global dataset of riverbank erosion for >370,000 kilometers of large rivers using 20 years of water classifications from Landsat imagery. We estimate uncertainty by propagating water classification errors through our methods. Globally, we find riverbank erosion for rivers wider than 150 m to have an approximately log-normal distribution with a median value of 1.52 m/yr. Comparing our dataset to 25 similar estimates of riverbank migration, we found an normalized mean absolute error of 42% but a bias of only 5.8%. We definitively show that river size is the best first-order predictor of riverbank erosion, in agreement with existing literature that used available data. We also show that the relationship between size and bank erosion is substantially different among a sample of global river basins and suggest that this is due to second-order influences of geology, hydrology, and human influence. These data will help improve models of sediment transport, support models of bank erosion, and improve our understanding of human modification of rivers.

Plain Language Summary

Riverbank erosion presents a serious risk to people and infrastructure. These risks are becoming increasingly hard to predict because of direct modification of the rivers by damming and bank stabilization, as well as indirect modification by climate change and land use change. Geomorphologists have developed scaling relationships based on watershed characteristics; however, these relationships are very coarse and limited by the available data. This research uses twenty

years of satellite imagery to develop the first global dataset of riverbank erosion, which both confirms existing knowledge and opens new avenues of research.

Introduction

Humans have long relied on rivers as a source fresh water, as a means of transportation, and because of their role in shaping the landscape. Our attraction to rivers consequently means people, buildings, and agriculture are at risk from riverbank erosion. For example, in Bangladesh, an estimated average of 60,000 people per year are displaced by riverbank erosion of the Ganges-Brahmaputra-Jamuna system (Mutton and Haque, 2004). In this context, it is easy to understand why the United States Army Corps of Engineers spends more than $200 million per year managing the Mississippi River (James, 2019). However, sediment deposition and riverbank accretion create natural riparian habitats and fertile floodplains (Florsheim et al., 2008). Humans are dramatically modifying river sedimentation, both directly through river management, infrastructure, and land use development (Shields et al., 2000; Kondolf et al., 2002), as well as indirectly through climate change (East and Sankey, 2020). Land development has greatly increased the total sediment transport of rivers, but trapping in reservoirs has resulted in a net reduction in sediment export from land (Syvitski et al., 2005). These changes in water and sediment supply alter riverbank migration rates as the morphology adjusts to the new conditions (Brandt, 2000). The deposition and erosion of material on the banks acts as a temporary store of sediment, attenuating the impact of changing sediment supply, and as such is an important input to sediment flux models (Kronvang et al., 2013). As we think about the consequences of human impacts on climate and the landscape, assessing large-scale patterns in geomorphology is becoming increasingly valuable (Grill et al., 2019).

The many applications and broad importance of riverbank erosion has resulted in diverse measurement methods. On annual timescales and local spatial scales, bank migration and channel sedimentation can be measured volumetrically with bank and bathymetry surveying techniques (e.g., De Rose and Basher, 2011). Tectonic geomorphologists collect sediment cores and use radiometric dating to relate sediment accumulation rates (which are largely transported and deposited by river processes) to mountain-building uplift processes over geologic time scales (e.g., Walling, 1999). Over annual to decadal time scales and large spatial scales, fluvial geomorphologists rely on remote sensing methods like repeat lidar and optical remote sensing (e.g., De Rose and Basher, 2011). Several methods have been developed to allow efficient analysis of large domains from satellite or aerial imagery (Peixoto et al., 2009; Monegaglia et al., 2018). Many of these methods find and track the movement of the river centerline, which works well for well-behaved single-threaded channels, but have difficulty representing the complexity of anabranching or braided rivers (Parker et al., 2011; Schwenk et al., 2017). Other approaches quantify bank migration by the area

that changes between river and non-river pixels (Rowland et al., 2016; Nagel et al., 2022). Because these methods calculate change on a pixel-by-pixel basis, they can more easily capture complex morphologies and irregular change that are not well represented by a river centerline. Among these many methods, there are also many ways to define riverbank migration; some consider only the erosion of stable, vegetated banks and bars (Boruah et al., 2008), while others include the shifting of channel bars (Lane et al., 2010). None of these methods have been used at global scales to produce a consistent dataset of riverbank migration across all climates and geographies. As a result, our existing geomorphological understanding of riverbank erosion and accretion are limited to, and biased by, the patchwork of studies and locations where we have observations.

Predicting and modeling bank erosion as a means of understanding sediment processes has a long history in geomorphology. Over that history, variables that describe the overall size of a river, such as catchment area, discharge, and width have all been found to be highly correlated with bank erosion (Hooke, 1980; Nanson and Hickin, 1986). River size is considered a "first order" control on bank migration (i.e. big rivers move faster than small rivers), and many researchers now investigate "second order" influences on bank erosion by first normalizing bank migration by the river width (Jarriel et al., 2021). Regardless of scale, we know from physical modelling that the rate of bank erosion is a balance between shear stress and bank resistivity (Ikeda et al., 1981). This balance points to second order controls that affect the interaction between flow and the banks. However, unlike the first order controls described above, the results of these studies are varied. For example, Constantine et al. (2014) found that suspended sediment flux is the primary control of width-normalized bank migration rate for 20 river reaches in the Amazon Basin. Ielpi and Lapôtre (2020) showed that the presence of vegetation slowed down width-normalized bank migration by an order of magnitude using a global sample of 983 meanders. Both of these variables can be heavily modified by human interventions, such as damming (Shields et al., 2000) and bank stabilization with concrete or vegetation (Grizzetti et al., 2017). These examples show the range of second order controls in the literature which arise from the different subsets of rivers studied. The interactions and hierarchies of these controls at the global scale have not yet fully been evaluated.

Here, we present the first global observations of decadal-scale average riverbank erosion and accretion for all rivers wider than 150 meters. We use a surface water occurrence dataset derived from Landsat satellite imagery, a river centerline dataset, and cloud computing to efficiently estimate decadal-scale average bank erosion and accretion rates. We analyze these data in the context of previous literature to show that existing methods of estimating riverbank erosion and accretion accurately capture large-scale patterns. However, the specific form of these relationships between geomorphic predictors and riverbank erosion and accretion varies from basin to basin. These data importantly confirm geomorphic scaling theories and present a new, uniform dataset that can help advance geomorphic modeling efforts.

Materials and Methods

Our data collection and processing are done entirely in the free, cloud-based geospatial platform Google Earth Engine (GEE) (Gorelick et al., 2017). GEE allows us to analyze large spatial datasets in the cloud without downloading the source imagery, which means our methods scale without having to manage storage or bandwidth issues. Our methods are optimized to run quickly on GEE's framework by calculating all change metrics using raster operations and then reducing the data to a table format before exporting. We used Python 3 and Geopandas for post processing and analysis of the vector data (Jordahl et al., 2021).

Water classification data

Accurate classification of water and land from satellite images is foundational to our calculations of bank migration. As such, we compare two widely used and validated water occurrence datasets based on the Landsat series of satellites. The first is the Joint Research Centre's (JRC) yearly water classification dataset, where each pixel is marked as either no data, not water, seasonal water, or permanent water (Pekel et al., 2016). Pixels marked seasonal water are pixels that were classified as water for at least one month but not every month with valid observations. The permanent water classification represents pixels that were observed to be water in all months with valid observations. We considered both permanent and seasonal water classifications for our binary water masks because permanent water classification is sensitive to omission errors and often results in disconnected river reaches. The other water classification dataset we use, by Pickens et al. (2020), is a classification tree model applied to the Landsat archive starting in 1999. Unlike the JRC dataset, each pixel in the yearly composites from the Pickens dataset represent the percentage of images that were classified as water. We selected a 70% occurrence threshold in the Pickens dataset which approximated the JRC seasonal and permanent classifications well. Visual inspection of this threshold showed stable river forms with minimal flooding or disconnected river reaches. The JRC dataset ranges from 1984 to 2020 at the time of writing and is currently updated annually. However, data are not equally available through time and space. Notably, some regions in northeast Siberia do not have any images before 1999 due to limited downlink capability and no on-board image storage on the Landsat-5 satellite. The launch of Landsat-7 in April 1999 increased spatial coverage when operating in tandem with Landsat-5 and included on-board image storage, enabling the capture of up to 10 scenes to be stored and transmitted later when the satellite was in range of a ground station (Goward et al., 2001). As such, we begin our analysis in 2000, when Landsat-7 records became fully available. Still, there are unavoidable problems with optical remote sensing that impact the quality and continuity of the Landsat record. Clouds, smoke, and the seasonal lack of sunlight at high latitudes can all limit the utility of images. Any dataset that uses optical satellite images, including the two water occurrence datasets used in this study, are prone

to incompleteness and biases because of these problems and limitations. Even so, temporal continuity and relatively high resolution make the Landsat archive the most viable satellite dataset for morphological analyses of the world's large rivers over time.

River data

We rely on the SWOT River Database (SWORD, Altenau et al., 2021) to inform our search area for river classification and to organize our pixel-level data into a vector product that includes river topology, unique identifiers, and other morphological variables. SWORD is based on the Global River Widths from Landsat dataset (Allen and Pavelsky, 2018) but with several improvements that increase the topological continuity, add additional reach identifiers that relate to other hydrographic datasets, and resample reaches to a more uniform length of approximately ten kilometers. Within each reach, the river is divided into nodes approximately every 200 meters that track the river centerline. We also use SWORD to filter small river reaches that we will not be able to reliably measure with Landsat. We limit migration calculations to river reaches with a mean width greater than 150 m, or approximately 5 Landsat pixels. We based this threshold on manual inspection of river classifications as well as our uncertainty estimates (section 2.5).

River identification

Rivers occupy only about 0.6% of earth's unglaciated land surface area, and as such, about the same percentage of pixels in satellite imagery (Allen and Pavelsky, 2018). We rely on the SWORD river centerline dataset to limit the scope of our search for rivers and greatly reduce the volume of pixels that we must process and classify. Identifying a river in a multispectral image or binary watermask is visually easy but often challenging with automated methods. In most environments, rivers display a unique shape and or color when compared to lakes in the floodplains. Rivers and lakes take on a wide range of morphologies, but, in general, rivers form sinuous channels that traverse long distances, whereas lakes are rounder and isolated. Identifying river pixels is often done by intersecting the river centerline with a watermask, such as in the RivWidthCloud algorithm (Yang et al., 2020). However, if the static centerline is inaccurate, whether by error or because of riverbank migration, using the intersection with a static centerline to identify the movement of rivers will often fail. Other approaches for identifying rivers include selecting polygons with high length to width ratios (Isikdogan et al., 2017) or polygons that intersect the edge of an image (Kyzivat et al., 2019). We combine these methods by selecting the polygon with the largest perimeter within the area buffered on the prior centerline dataset. We buffer the river centerline by 10 rivers widths, which approximates the meander amplitude (Leuven et al., 2018), and thus the approximate maximum distance the channel will move before reversing direction. Selecting the largest polygon by perimeter would identify many lakes and reservoirs in a global search, but we

largely avoid this issue by limiting our search to the area within 10 river widths of the static river centerline and by excluding any pixels that are included in the HydroLakes dataset (Messager et al., 2016). These methods allow us to produce global annual maps of river pixels from 2000-2021 suitable for detection of bank migration over time.

Bank Migration

We use an area-based approach to quantifying riverbank erosion and accretion, similar to the SCREAM method from Rowland et al., (2016). This approach is advantageous for global applications because it can better represent multi-threaded rivers than centerline-based methods do, and raster operations are much faster than vector operations in GEE. We measured riverbank erosion and accretion by comparing river inundation masks from different years and counting the pixels that transition between river and land. Pixels that transition from river to land are marked as accretion, and pixels that transition from land to river are marked as erosion (Figure 1b). Our first step is to calculate the area and bank characteristics of the individual images. We locate the bank pixels by dilating the river mask by one pixel, subtracting the original river mask, and then calculate the bank aspect by convolving the bank pixels with a directional kernel (Figure 1c). We measure the standard deviation of local bank aspect as a proxy for bank curvature for each side of the banks. Measuring bank curvature typically uses the radius of a best fit circle for a section of river, which is a slow process in the GEE framework. Next, we calculate the pixel-scale magnitude and direction of change using the same methods in Rowland et al. (2016; Figure 1d). The magnitude of erosion is calculated for each bank pixel in the first image as the shortest path to any of the bank pixels in the second image, where each path is constrained to only traverse pixels that were eroded. For islands and bars that have entirely eroded, the distance is calculated from the island perimeter to the island centroid. The result of these distance calculations is a raster surface that slopes between the banks in the two images, and we use the gradient of this surface to calculate the direction of erosion. Accretion is calculated in the same manner with the images switched and the paths constrained to the accreted area. These change metrics are relatively simple, efficient to calculate, and describe the change in pixel-by-pixel detail. While the raster data preserve all the detail in the original river masks and our change calculations, that fidelity comes with high cost when exporting and analyzing the data. We exported this data only in limited cases while developing the methods and visualizing the results over small regions and are not available globally.

To produce the structured global river erosion data product we summarize the raster data to a vector product by reducing the pixels to their nearest river centerline node in SWORD (Figure 1e). In our final data, the vector dataset includes the original SWORD hydrography data (centerline location, upstream and downstream connections, Pfafstetter basin codes, flow accumulation values,

slope, mean width, sinuosity, etc.) and a summary of the change calculations (total river area in time 1 and time 2, accreted area, eroded area, average rate of change, average direction of change, variance in direction, and uncertainty estimates) at >2.2 million nodes spaced approximately 200 m apart. We further aggregate the data up to the reach and watershed scales for analysis, which allows flexibility in future analysis. For example, while we present average bank migration values at large scales, others may be interested in the maximum value for a particular reach. The high-resolution node data also allows for resampling the data over custom reaches and extents, beyond the reach and basin structure in SWORD.
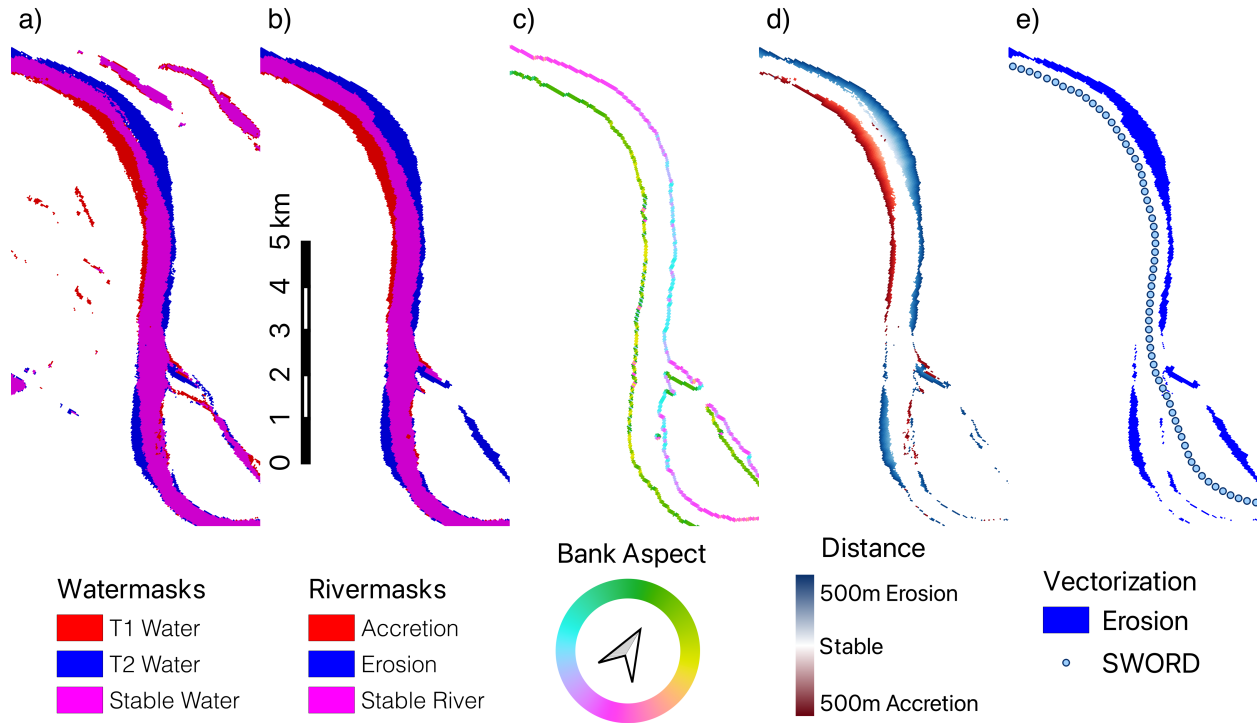

Figure 1. a) Overlapping watermasks from two years in red and blue; purple indicates pixels classified as river in both years. b) Rivermasks produced from the watermasks after identifying river pixels and a closure operation. c) Bank aspect (only one image is shown, and the bank pixels are dilated for visibility). d) distance or magnitude of change for all river pixels that eroded or accreted. e) The SWORD centerline overlain on erosion pixels. During vectorization, each pixel is assigned to the closest river centerline node and a summary of geomorphic change is calculated for each centerline node.

Uncertainty

We first quantify the uncertainty of our estimates by propagating the water classification errors through our methods. Both the JRC and Pickens datasets include classification error rates. For the JRC dataset, omission and commission errors are estimated for each seasonality class (seasonal or permanent) and sensor (Landsat 5, 7, or 8). Errors are highest in the seasonal omission category, and lowest in the permanent commission for all sensors. There is not as large of a difference between sensors, however the downlink capability during Landsat 5 was limited, and the scan line corrector failure on Landsat 7 limits the quality of the seasonality classifications. The Pickens dataset takes a different approach, quantifying the omission and commission error rates as a function of distance from the land-water boundary for both the Pickens and JRC datasets. We use these distanced-based uncertainties for both datasets because we believe they better represents the sources and patterns of error and uncertainty in classifications. Further, the seasonality classifications in the JRC dataset do not validate well against the high-resolution, manually trained and classified validation data from Pickens et al. (2020).

We apply these error rates to the annual water masks by randomly adding omission and commission errors according to the distance-rate function in Pickens et al., (2020). We repeat this process according to the number of observations in each annual watermask and then average the erroneous watermasks together, simulating the effect of the per image pixel-scale errors to the annual water masks (Figure S1). Each time we analyze two images for change detection, we also create two noisy watermasks and process them with the same river classification and change analysis methods (sections 2.3 & 2.4). The difference between our 'clean' watermasks and the 'noisy' watermasks is a quantification of the erroneous planform change we would anticipate given no actual change in planform (Figure S2).

Another source of uncertainty stems from variations in river stage. When looking at water surfaces only in planform, changes in inundation cannot be distinguished from changes in channel form. For example, if we happen to observe a flood in year one and low flows in year two, our bank migration data could suggest accretion along both banks. We reduce this source of error by using the composited annual masks, though interannual variability will still be present in our data. We investigate the severity of interannual variation by performing our calculations on 9 combinations of years, in a 3x3 matrix of years from 2000-2002 compared to 2017-2019 (Figure S3). Our final dataset incorporates these data by presenting the minimum, maximum, and median riverbank erosion and accretion values for each node.
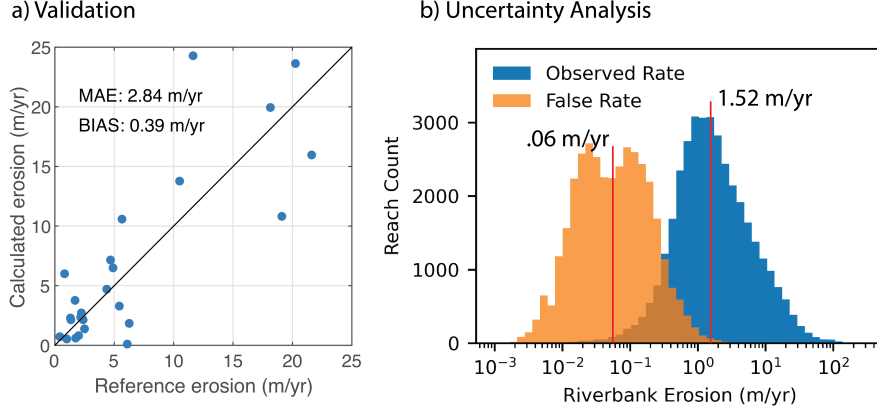
Validation

To assess the accuracy of our riverbank migration estimates, we calculated the bank erosion rate for river reaches where previous studies have published rates

of erosion. After filtering the dataset of 290 published studies (Rowland and Schwenk, 2019) down to studies that obtain similar metrics (producing reach-averaged rates and over decade-scale time intervals) and wider than 150 meters, there are 25 cases remaining (See supplemental S4 for a map of validation sites and Supplemental T1 for full list of references and reach characteristics). We limit the validation studies to decade-scale measurements because year-to-year variations in discharge and erosion can bias or misrepresent the characteristic erosion rate when the time scale of observations changes (Donovan et al., 2019). Further, any change in erosion rate over time could falsely add error to the validation, so we exclude studies with data collection that ended before our satellite record. The reach definition is not identical between the published studies and our data so we compared the migration rate for each validation reach to our observed migration rate nearest the reported validation reach center.

Results

Our data compare very well to the 25 validation reaches, with a mean absolute error of 2.84 meters per year and a bias of 0.39 meters per year (Figure 2a). Unfortunately these limited validation sites are not equally distributed around the world and do not represent a very broad range of morphologies (Figure S5). Nevertheless, our validation results suggest that our method and implementation in GEE can capture riverbank erosion with similar accuracy to studies focused on smaller domains.

The results of our classification uncertainty analysis show that the global median bank migration rate (1.52 m/year) is more than an order of magnitude higher than the median false erosion rate associated with pixel misclassification error (.06 m/year). The distribution of the observed riverbank migration rate is approximately log normal, while false erosion rate is slightly bimodal when binned in log scale (Figure 2b). Of course, it is not true that the bank migration rate is an order of magnitude higher than the false erosion rate everywhere, in fact many reaches with low migration rates will have nearly equivalent rates of false migration. 5.7% of reaches have false erosion rates higher than their median observed bank erosion rate. Narrow rivers and anabranching rivers have more bank pixels per unit length than wide single channel rivers, and as such will have higher average rates of classifcation errors. The uneven distribution of Landsat images also greatly biases the false erosion estimates, as areas with fewer images have higher rates of classifcation errors in the annual watermask products (Figure

a) Validation

b) Uncertainty Analysis

Figure 2. a) Validation of the riverbank erosion from REAL (vertical axis) with references from literature (horizontal axis). b) The distribution of global observed riverbank erosion rate is shown in blue. The false erosion rate is shown in orange and indicates the uncertainty from water classification errors.

S3).

Our global estimates of riverbank migration are mapped in Figure 3a after averaging the data to Pfaffstetter level 6 basins. At the largest scales, these data agree with our expectations: rivers like the Amazon, Orinoco, Paraná, Mississippi, Syr Darya, Indus, Ganges-Brahmaptura-Meghna (GBM), Yangtze, and Niger show very high rates of erosion. In contrast, rivers in Europe, much of Siberia, and the Canadian Shield show low average rates of bank migration. European rivers have been modified and stabilized since at least the 16th century to serve the people that live near them, and as such show very low rates of riverbank migration (Evette et al., 2009; Grizzetti et al., 2017). The Canadian Shield region also shows near-zero riverbank migration rates, but for very different reasons. Rivers in the Candian Shield region are not heavily modified by humans, but flow over highly resistive precambrian igneous and metamorphic rock. Large swaths of the Arctic show low migration rates, with some notable exceptions in the Russian Far East, Northern Siberia, and parts of the Yukon River.

At finer scales we can see intrabasin and reach scale patterns. Within the Amazon basin, the subbasins coming off of the Andes mountains show the highest rates of erosion, while tributaries from the central trough are more stable (Figure 3b). Upon closer inspection, and aggregated to the 10km SWORD reaches, we can see high variability in bank erosion between reaches, with a distinct drop in erosion downstream of a confluence with a tributary (Figure 3c). Visual inspection of satellite images suggests that this tributary (Ituxi River) typically

has lower sediment concentrations than the Purus River. At the finest scale of REAL, the 200m node spacing, we see meander-scale sediment processes on the Purus River (Figure 3d). Nodes near the apex of the meander bends typically show high rates of erosion, while the straight connecting sections show much lower rates of erosion. We also see a pattern of high rates of erosion before and after the apex of the bend, indicating the expected positive bias in erosion on the downstream bank faces.

a)

Riverbank
Erosion (m/yr)

>20

10

0

b) Pfafstetter 6

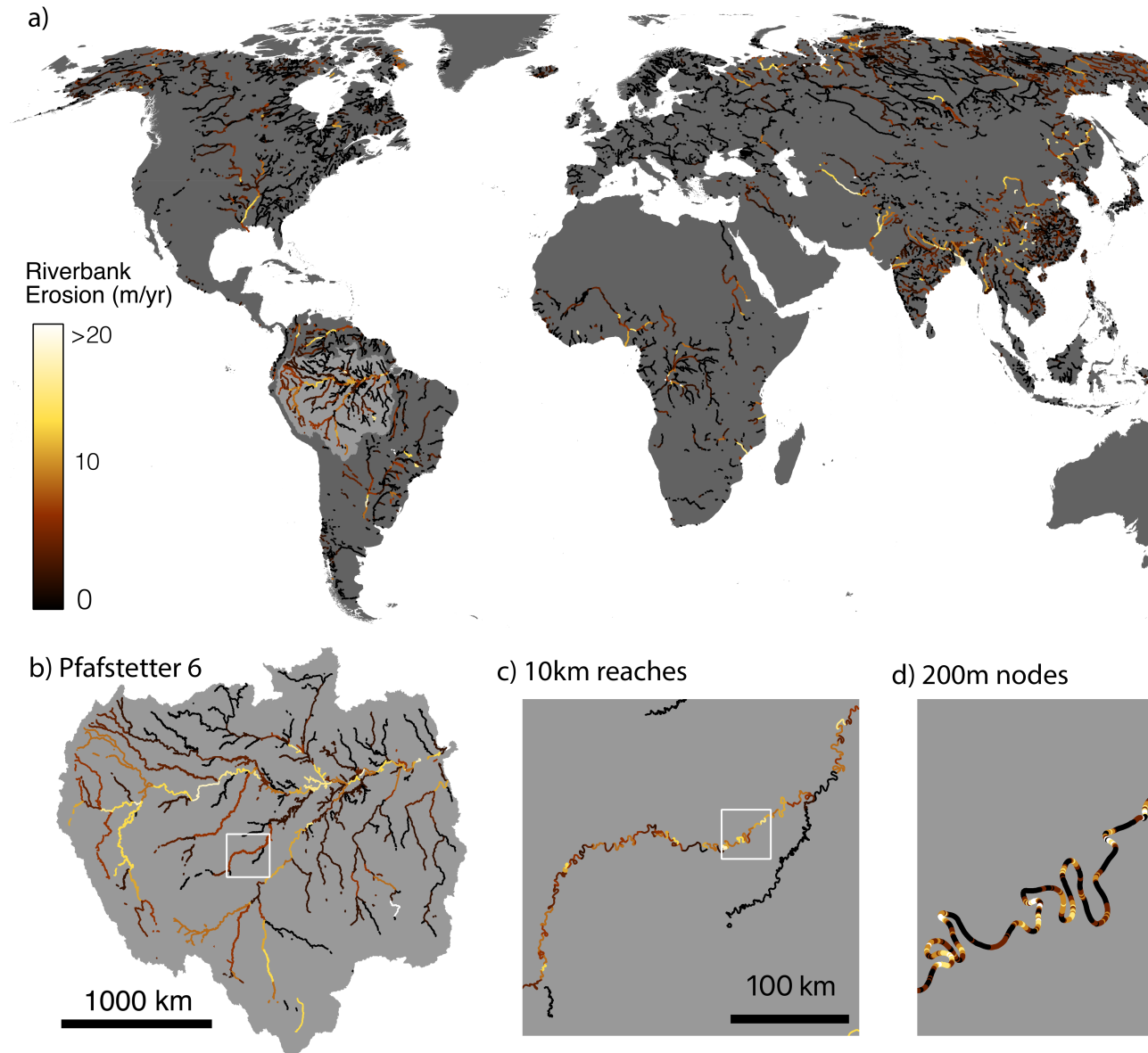c) 10km reaches

d) 200m nodes

1000 km

100 km

Figure 3. a) Global riverbank erosion rates averaged at Pfafstetter level 6 basins. b) Amazon basin inset showing Pfafstetter level 6 averages. c) reach averages using the approximately 10 km reaches in SWORD. d) The finest scale of REAL data shown for a section of the Purus River, node data spaced approximately every 200m.

Beyond the broad, global scale spatial patterns there is a lot of potential analysis with regards to inter- and intra-basin relationships. We show scatterplots of river width versus the observed bank erosion rate for the 16 basins with the most valid observations to investigate the first order scaling relationships (Figure 4). Generally, the relationships show a spectrum from highly linear (e.g. Ganges-Brahmputra-Meghna) to weak relationships and clustered values near the low end of width and erosion rate (e.g. Yangtze and Yenisei). In comparison to the global relationship proposed by Hooke (1982) shown in dark red, some basins approximate this relationship well (e.g. Amazon and Paraná), while several notable river basins are biased low (e.g. Congo, Ob', and Yukon).
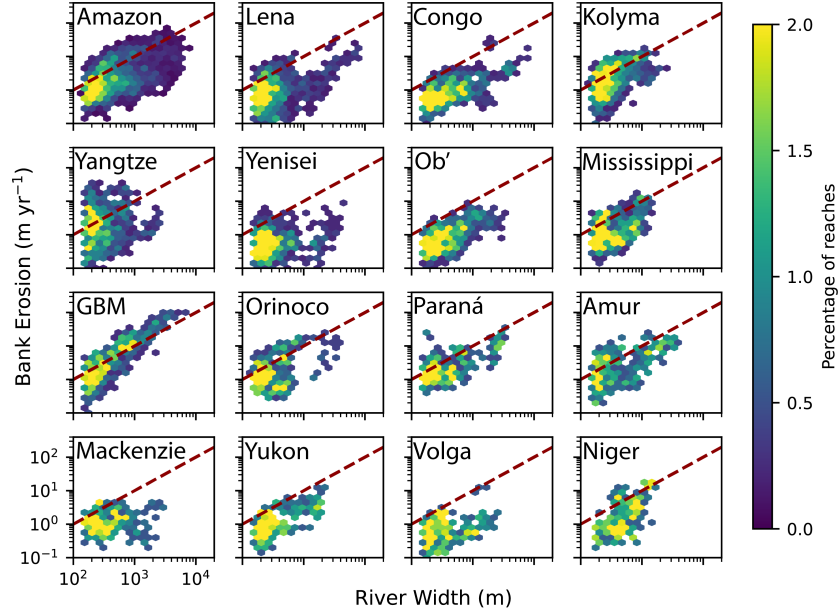

Figure 4. Relationships between reach-averaged meander rate and width for Pfafstetter level 3 river basins. The color of each hexagonal bin represents the percent of all observed reaches in that basin that are within the bounds of that bin. "GBM" refers to the Ganges-Brahmaputra-Meghna river basin. The dark red dashed line represents the $M = 0.01W$ relationship proposed by Hooke (1982) as an first-order estimate of riverbank erosion.

Discussion and Conclusion

Our results suggest that previous regional studies indicating that size is the first order control on riverbank erosion at large scales (Hooke, 1980; Nanson and Hickin, 1986; Ielpi and Lapôtre, 2020) are largely correct (e.g. Figure 4). However, upon closer inspection, we reveal the limits of the global applicability of such relationships. We show large regional differences in this first order relationship that arise from the unique blend of secondary controls in each basin. For example, riverbank erosion in the Congo basin, which is characterized by varied drainage patterns due to localized geologic controls (Flügel et al., 2015), is notably lower than the global average. The world's largest basin by discharge, the Amazon, has a lot of spread in this first order relationship, a result of the varied inputs of sediment load as shown by Constantine et al. (2014) and seen in the REAL data in Figure 4b. The Ob' basin is also biased low, however, likely due to low flows in the winter and a discontinuous and sporadic permafrost setting. On the other hand, riverbank erosion in the Ganges-Brahmputra-Meghna basin is higher than the global average, which may be because of high relief and sediment yield in the tectonically active headwaters and thick alluvium downstream as well as frequent high discharge during monsoon season. As shown in these examples, river size does provide a good first order approximation of riverbank erosion for most basins globally, however these specific relationships can vary greatly between regions. REAL provides a starting point for analyzing these second order relationships at the global scale, and further research may be able to show the relative importance of geologic, hydrologic, and human influences on the rate of riverbank erosion in different basins.

We have revealed and clarified some limitations in quantifying river planform change using remotely sensed data products. First, the resolution of Landsat (~30 meters) requires decades between images to reliably detect the rate of change for all but the most dynamic rivers. This long timeframe comes with an added challenge, in that any changes in hydrology, human influence, or data quality over the intervening years can result in biased estimates of planform change. Higher resolution satellites like Sentinel-2 and the Planet constellation will become increasingly viable for global riverbank migration analysis as the length of record grows, and at the very least would be useful for multi-source remote sensing data fusion with the Landsat record. Second, the uncertainty in water classifications is a well-known problem in remote sensing of planform change, however the severity of the problem is in relation to the magnitude of actual planform change. We found that classification uncertainties propagated through our change calculations were greater than the observed planform change for only about 5.7% of rivers. Improving the representation of all sources of uncertainty and the impact on change calculations is a necessary next step remote sensing of river morphology change detection.

We have also provided the first global accounting of highly mobile rivers that may present a problem to remote sensing applications which treat rivers as immobile. Our earth observation satellite record is now several decades long,

yet most river morphology data are static in time. As the satellite record grows, dynamic methods that track the movement and change of rivers in time will be critical. Even satellite missions over relatively short periods, like the SWOT satellite (Biancamaria et al., 2016), which is currently planned to launch in 2022 and will be operational for 3 years, will require some flexibility to accommodate the mismatch between SWORD centerline locations and highly mobile rivers. The REAL dataset provides the historical data to predict where and how soon these problems may arise in the future.

Acknowledgments

Open Research

The annual water classification data used to identify permanent water bodies are available in the original publication and via https://www.glad.umd.edu/dataset. SWORD, the river centerline dataset used to separate rivers from lakes and other surface water, is available online in netCDF and shapefile formats via https://zenodo.org/record/3898570. The REAL dataset will be available via Zenodo upon publication in shapefile and csv formats. Additionally, the data can be viewed online in a Google Earth Engine Application at https://tedlanghorst.users.earthengine.app/view/realnodes.

References

Allen, G.H., and Pavelsky, T., 2018, Global extent of rivers and streams: Science, v. 361, p. 585–588, doi:10.1126/science.aat063.Altenau, E.H., Pavelsky, T.M., Durand, M.T., Yang, X., Frasson, R.P. de M., and Bendezu, L., 2021, The Surface Water and Ocean Topography (SWOT) Mission River Database (SWORD): A Global River Network for Satellite Data Products: Water Resources Research, v. 57, p. 1–15, doi:10.1029/2021WR030054.Biancamaria, S., Dennis Lettenmaier, B.P., and Tamlin Pavelsky, B.M., 2016, The SWOT Mission and Its Capabilities for Land Hydrology: Surveys in Geophysics, v. 37, p. 307–337, doi:10.1007/s10712-015-9346-y.Boruah, S., Gilvear, D., Hunter, P., and Nayan, S., 2008, QUANTIFYING CHANNEL PLANFORM AND PHYSICAL HABITAT DYNAMICS ON A LARGE BRAIDED RIVER USING SATELLITE DATA—THE BRAHMAPUTRA, INDIA SANCHITA: River Research and Applications, p. 650–660, doi:10.1002/rra.Brandt, S.A., 2000, Classification of geomorphological effects downstream of dams: Catena, v. 40, p. 375–401, doi:10.1016/S0341-8162(00)00093-X.Constantine, J.A., Dunne, T., Ahmed, J., Legleiter, C., and Lazarus, E.D., 2014, Sediment supply as a driver of river meandering and floodplain evolution in the Amazon Basin: Nature Geoscience, v. 7, p. 899–903, doi:10.1038/ngeo2282.Donovan, M., Belmont, P., Notebaert, B., Coombs, T., Larson, P., and Souffront,

M., 2019, Accounting for uncertainty in remotely-sensed measurements of river planform change: Earth-Science Reviews, v. 193, p. 220–236, doi:10.1016/j.earscirev.2019.04.009.East, A.E., and Sankey, J.B., 2020, Geomorphic and Sedimentary Effects of Modern Climate Change: Current and Anticipated Future Conditions in the Western United States: Reviews of Geophysics, v. 58, doi:10.1029/2019RG000692.Evette, A., Labonne, S., Rey, F., Liebault, F., Jancke, O., and Girel, J., 2009, History of bioengineering techniques for erosion control in rivers in western europe: Environmental Management, v. 43, p. 972–984, doi:10.1007/s00267-009-9275-y.Florsheim, J.L., Mount, J.F., and Chin, A., 2008, Bank Erosion as a Desirable Attribute of Rivers: BioScience, v. 58, p. 519–529, doi:10.1641/b580608.Flügel, T.J., Eckardt, F.D., and Cotterill, F.P.D., 2015, The Present Day Drainage Patterns of the Congo River System and their Neogene Evolution, *in* Geology and resource potential of the Congo basin, Springer, p. 315–337, doi:10.1201/9781315161808-4.Gorelick, N., Hancher, M., Dixon, M., Ilyushchenko, S., Thau, D., and Moore, R., 2017, Google Earth Engine: Planetary-scale geospatial analysis for everyone: Remote Sensing of Environment, doi:10.1016/j.rse.2017.06.031.Goward, S.N., Masek, J.G., Williams, D.L., Irons, J.R., and Thompson, R.J., 2001, The Landsat 7 mission: Terrestrial research and applications for the 21st century: Remote Sensing of Environment, v. 78, p. 3–12, doi:10.1016/S0034-4257(01)00262-0.Grill, G. et al., 2019, Mapping the world's free-flowing rivers: Nature, v. 569, p. 215–221, doi:10.1038/s41586-019-1111-9.Grizzetti, B., Pistocchi, A., Liquete, C., Udias, A., Bouraoui, F., and Van De Bund, W., 2017, Human pressures and ecological status of European rivers: Scientific Reports, v. 7, p. 1–11, doi:10.1038/s41598-017-00324-3.Hooke, J.M., 1980, Magnitude and distribution of rates of river bank erosion.: Earth Surface Processes, v. 5, p. 143–157, doi:10.1002/esp.3760050205.Ielpi, A., and Lapôtre, M.G.A., 2020, A tenfold slowdown in river meander migration driven by plant life: Nature Geoscience, v. 13, doi:10.1038/s41561-019-0491-7.Ikeda, S., Parker, G., and Sawai, K., 1981, Bend theory of river meanders. Part 1. Linear development: Journal of Fluid Mechanics, v. 112, p. 363–377, doi:10.1017/S0022112081000451.Isikdogan, F., Bovik, A., and Passalacqua, P., 2017, RivaMap: An automated river analysis and mapping engine: Remote Sensing of Environment, v. 202, p. 88–97, doi:10.1016/j.rse.2017.03.044.James, R.D., 2019, Civil Works Budget of the U.S. Army Corps of Engineers.:Jarriel, T., Swartz, J., and Passalacqua, P., 2021, Global rates and patterns of channel migration in river deltas: Proceedings of the National Academy of Sciences of the United States of America, v. 118, doi:10.1073/pnas.2103178118.Jordahl, K. et al., 2021, Geopandas:, doi:10.5281/zenodo.4569086.Kondolf, G.M., Piégay, H., and Landon, N., 2002, Channel response to increased and decreased bedload supply from land use change: Contrasts between two catchments: Geomorphology, v. 45, p. 35–51, doi:10.1016/S0169-555X(01)00188-X.Kronvang, B., Andersen, H.E., Larsen, S.E., and Audet, J., 2013, Importance of bank erosion for sediment input, storage and export at the catchment scale: Journal of Soils and Sediments, v. 13, p. 230–241, doi:10.1007/s11368-012-0597-7.Kyzivat, E.D. et al., 2019, A high-resolution airborne color-infrared

camera water mask for the NASA ABoVE campaign: Remote Sensing, v. 11, doi:10.3390/rs11182163.Lane, S.N., Widdison, P.E., Thomas, R.E., Ashworth, P.J., Best, J.L., Lunt, I.A., Sambrook Smith, G.H., and Simpson, C.J., 2010, Quantification of braided river channel change using archival digital image analysis: Earth Surface Processes and Landforms, v. 35, p. 971–985, doi:10.1002/esp.2015.Leuven, J.R.F.W., van Maanen, B., Lexmond, B.R., van der Hoek, B. V., Spruijt, M.J., and Kleinhans, M.G., 2018, Dimensions of fluvial-tidal meanders: Are they disproportionally large? Geology, v. 46, p. 923–926, doi:10.1130/G45144.1.Messager, M.L., Lehner, B., Grill, G., Nedeva, I., and Schmitt, O., 2016, Estimating the volume and age of water stored in global lakes using a geo-statistical approach: Nature Communications, v. 7, p. 1–11, doi:10.1038/ncomms13603.Monegaglia, F., Zolezzi, G., Güneralp, I., Henshaw, A.J., and Tubino, M., 2018, Automated extraction of meandering river morphodynamics from multitemporal remotely sensed data: Environmental Modelling & Software, v. 105, p. 171–186.Mutton, D., and Haque, C.E., 2004, Human Vulnerability, Dislocation and Resettlement: Adaptation Processes of River-bank Erosion-induced Displacees in Bangladesh: Disasters, v. 28, p. 41–62, doi:10.1111/j.0361-3666.2004.00242.x.Nagel, G.W., de Moraes Novo, E.M.L., Martins, V.S., Campos-Silva, J.V., Barbosa, C.C.F., and Bonnet, M.P., 2022, Impacts of meander migration on the Amazon riverine communities using Landsat time series and cloud computing: Science of the Total Environment, v. 806, p. 150449, doi:10.1016/j.scitotenv.2021.150449.Nanson, G.C., and Hickin, E.J., 1986, A statistical analysis of bank erosion and channel migration in western Canada.: Geological Society of America Bulletin, v. 97, p. 497–504, doi:10.1130/0016-7606(1986)97<497:ASAOBE>2.0.CO;2.Parker, G., Shimizu, Y., Wilkerson, G. V., Eke, E.C., Abad, J.D., Lauer, J.W., Paola, C., Dietrich, W.E., and Voller, V.R., 2011, A new framework for modeling the migration of meandering rivers: Earth Surface Processes and Landforms, v. 36, p. 70–86, doi:10.1002/esp.2113.Peixoto, J.M.A., Nelson, B.W., and Wittmann, F., 2009, Spatial and temporal dynamics of river channel migration and vegetation in central Amazonian white-water floodplains by remote-sensing techniques: Remote Sensing of Environment, v. 113, p. 2258–2266, doi:10.1016/j.rse.2009.06.015.Pekel, J.F., Cottam, A., Gorelick, N., and Belward, A.S., 2016, High-resolution mapping of global surface water and its long-term changes: Nature, v. 540, p. 418–422, doi:10.1038/nature20584.Pickens, A.H., Hansen, M.C., Hancher, M., Stehman, S. V., Tyukavina, A., Potapov, P., Marroquin, B., and Sherani, Z., 2020, Mapping and sampling to characterize global inland water dynamics from 1999 to 2018 with full Landsat time-series: Remote Sensing of Environment, v. 243, p. 111792, doi:10.1016/j.rse.2020.111792.De Rose, R.C., and Basher, L.R., 2011, Measurement of river bank and cliff erosion from sequential LIDAR and historical aerial photography: Geomorphology, v. 126, p. 132–147, doi:10.1016/j.geomorph.2010.10.037.Rowland, J.C., and Schwenk, J., 2019, Global meta-analysis of published river bank erosion and migration rates:, doi:10.15485/1571181.Rowland, J.C., Shelef, E., Pope, P.A., Muss, J., Gangodadamage, C., Brumby, S.P., and Wilson, C.J., 2016, A morphology

independent methodology for quantifying planview river change and characteristics from remotely sensed imagery: Remote Sensing of Environment, v. 184, p. 212–228, doi:10.1016/j.rse.2016.07.005.Schwenk, J., Khandelwal, A., Fratkin, M., Kumar, V., and Foufoula-Georgiou, E., 2017, High spatiotemporal resolution of river planform dynamics from landsat: The rivMAP toolbox and results from the Ucayali river: Earth and Space Science, v. 4, p. 46–75, doi:10.1002/2016EA000196.Shields, F.D., Simon, A., and Steffen, L.J., 2000, Reservoir effects on downstream river channel migration: Environmental Conservation, v. 27, p. 54–66, doi:10.1017/S0376892900000072.Syvitski, J.P.M., Vörösmarty, C.J., Kettner, A.J., and Green, P., 2005, Impact of Humans on the Flux of Terrestrial Sediment to the Global Coastal Ocean: Science, v. 308, p. 376–381.Walling, D.E., 1999, Linking land use, erosion and sediment yields in river basins: Hydrobiologia, v. 410, p. 223–240, doi:10.1023/A:1003825813091.Yang, X., Pavelsky, T.M., Allen, G.H., and Donchyts, G., 2020, RivWidthCloud: An Automated Google Earth Engine Algorithm for River Width Extraction from Remotely Sensed Imagery: IEEE Geoscience and Remote Sensing Letters, v. 17, p. 217–221, doi:10.1109/LGRS.2019.2920225.